

THE CDF IIb DETECTOR
TECHNICAL DESIGN REPORT

The CDF IIb Collaboration

August 2002

Contents

1	Overview	1-1
1.1	Introduction	1-1
1.2	History	1-1
1.3	Accelerator Configuration for Run IIb	1-2
1.4	The CDF II Detector	1-2
1.4.1	Tracking Systems	1-2
1.4.2	Calorimeter Systems	1-7
1.4.3	Muon Systems	1-7
1.4.4	Electronics and Triggering	1-7
1.5	The CDF II Upgrade Plan	1-9
1.5.1	Outlook	1-10
2	Physics Goals	2-1
2.1	Overview	2-1
2.1.1	Higgs Boson Physics	2-1
2.1.2	Properties of the Top Quark	2-2
2.1.3	A Precision Electroweak Program	2-2
2.1.4	Search for New Phenomena	2-2
2.1.5	Precision QCD at Large Q^2	2-3
2.1.6	Constraining the CKM Matrix	2-3
2.1.7	Detailed Discussion	2-3
2.2	Higgs physics in Run 2b	2-4
2.2.1	Standard Model Higgs	2-4
2.2.2	Low-mass Higgs	2-4
2.2.3	High-mass Higgs	2-5
2.2.4	SM Higgs Reach in Run 2	2-5
2.2.5	SUSY Higgs	2-7
2.2.6	Summary	2-8
2.3	Properties of the Top Quark	2-11
2.3.1	Review of Run I Analysis	2-11
2.3.2	Lessons from Run I	2-15
2.3.3	Impact of Upgrades on Top Physics	2-16
2.3.4	Event Yield	2-17
2.3.5	Measurement of the Top Quark Mass	2-18
2.3.6	Production Cross Section, $\sigma_{t\bar{t}}$	2-18
2.3.7	Measurement of a $t \rightarrow W$ Branching Fraction	2-19
2.3.8	Measurement of a $t \rightarrow b$ Branching Fraction	2-19
2.3.9	Anomalous Couplings and Weak Universality	2-19
2.3.10	Single Top Quark Production	2-21

2.3.11	Search for Anomalously Large Rare Decays	2-22
2.3.12	Summary of Top Physics	2-23
2.4	Precision Electroweak Program	2-28
2.4.1	Introduction	2-28
2.4.2	Impact of Proposed Run IIb Upgrades	2-28
2.4.3	W Mass	2-29
2.4.4	W Width	2-34
2.4.5	Gauge Boson Couplings	2-35
2.4.6	Forward-Backward Z Asymmetry	2-36
2.5	Search for New Phenomena	2-41
2.5.1	Introduction	2-41
2.5.2	Generic exotic signatures and the CDF II upgrade	2-41
2.5.3	Illustrative signatures in specific models	2-43
2.5.4	Detecting long-lived, massive particles	2-48
2.5.5	Summary	2-52
2.6	QCD	2-57
2.6.1	Introduction	2-57
2.6.2	Inclusive Jets	2-58
2.6.3	α_s and PDFs	2-60
2.6.4	Exploring High x	2-60
2.6.5	W and Z production	2-61
2.6.6	Single and Double Photon Production	2-63
2.6.7	Diffraction Physics	2-64
2.7	B Physics in Run IIb	2-70
2.7.1	Introduction	2-70
2.7.2	The Run I CDF b program	2-70
2.7.3	CDF strategy for b physics in Run II	2-71
2.7.4	Plans for Run IIb	2-72
2.7.5	CP Violation in the B system	2-73
2.7.6	Mixing and Lifetime Differences	2-79
2.7.7	B _c ⁺ Decays	2-80
2.7.8	Rare B decays	2-81
2.7.9	Radiative B Decays	2-82
2.7.10	Semileptonic Decays	2-83
2.7.11	$\psi(2S)$ Polarization	2-83
2.7.12	Concluding remarks	2-84

3	Run IIb Silicon Vertex Detector (SVX IIb)	3-1
3.1	Introduction	3-1
3.1.1	Conceptual Design	3-2
3.1.2	Schedule	3-3
3.2	Mechanical Layout	3-5
3.2.1	Overview	3-5
3.2.2	Stave (ladder) Design	3-7
3.2.3	Beampipe	3-10
3.2.4	Bulkheads	3-10
3.2.5	Spacetube	3-11
3.2.6	Barrel Assembly and Installation	3-11
3.2.7	Alignment with the Beam Axis	3-11
3.2.8	Secondary Vertex Trigger (SVT)	3-15

3.2.9	Alignment	3-15
3.2.10	Position Monitoring	3-16
3.3	Cooling and Gas systems	3-16
3.3.1	Stave Cooling	3-17
3.4	Sensors and fine-pitch cables	3-18
3.4.1	Radiation damage	3-18
3.4.2	Sensor Specifications	3-22
3.4.3	Inner Layer Lightweight Cables	3-23
3.5	Data Acquisition	3-23
3.5.1	Introduction	3-23
3.5.2	Readout times	3-24
3.5.3	Hybrids and Staves	3-26
3.5.4	Mini Port-card	3-28
3.5.5	Junction Port Cards (JPC)	3-32
3.5.6	Cables	3-32
3.5.7	FTM's and associated modules	3-32
3.5.8	Power Supplies	3-33
3.5.9	Failure Mode Analysis	3-33
3.5.10	Summary	3-35
3.6	SVX4 Chip	3-35
3.7	Material	3-41
3.8	Descoping	3-44
3.9	Summary	3-44
4	Silicon Detector Design	4-1
4.1	Detector Layout	4-1
4.2	Impact Parameter Resolutions	4-2
4.3	Double axial tracking layers	4-3
4.4	Tracking in the stereo view	4-4
4.5	Innermost Layer Placement	4-6
4.6	Pattern Recognition Efficiency	4-8
4.7	Descoping	4-10
4.8	Conclusions	4-12
5	Calorimetry	5-1
5.1	Introduction	5-1
5.2	Central Preshower Detector	5-1
5.2.1	Introduction	5-1
5.2.2	Run I Physics Using the CPR and CCR	5-1
5.2.3	Occupancy Issues	5-2
5.2.4	Upgraded Detector Design for Run IIb	5-4
5.3	Electromagnetic Calorimeter Timing	5-6
5.3.1	Introduction	5-6
5.3.2	Searching for New Physics with Photons	5-7
5.3.3	The EMTiming Project	5-9
5.3.4	Summary and Conclusions	5-14

6	Run I Ib Trigger & Data Acquisition Upgrades	6-1
6.1	Introduction	6-1
6.2	System Requirements	6-1
6.2.1	Luminosity Design Guidelines	6-1
6.2.2	CDF Triggers for Run I Ib	6-1
6.3	TDC Upgrade	6-2
6.3.1	TDC Specifications	6-2
6.3.2	TDC Technical Design	6-3
6.4	XFT Upgrade	6-5
6.4.1	Introduction	6-5
6.4.2	XFT Performance: Current and Extrapolated	6-6
6.4.3	Expected Performance of an Upgraded XFT	6-9
6.4.4	Upgrade XFT System Overview	6-12
6.4.5	The XTC Module	6-14
6.4.6	XTC To Finder Transmission	6-14
6.4.7	Finder Module Design	6-14
6.4.8	Finder To Linker Transmission	6-18
6.4.9	Linker Module Design	6-18
6.4.10	Linker TO XTRP Transmission	6-20
6.4.11	XFT Stereo Segment Finding	6-20
6.4.12	Stereo Segment Linking	6-22
6.4.13	The Track Trigger 3D	6-23
6.4.14	Timing	6-23
6.5	SVT Upgrade	6-23
6.6	Level 2 Decision Crate Upgrade	6-24
6.7	Event-Builder and Level-3	6-25
6.7.1	Limitations of the Existing System	6-26
6.7.2	Event-Builder Maintenance and Upgrade	6-28
6.7.3	System Maintenance	6-28
6.7.4	Upgrading the ATM Network	6-28
6.7.5	Level-3 PC Farm Upgrade	6-29
6.7.6	Event Builder/Level 3 Upgrades: Conclusions	6-29
7	Installation	7-1
8	Publications	8-1

Chapter 1

Overview

1.1 Introduction

The physics program at the Fermilab Tevatron Collider will continue to explore the high energy frontier of particle physics until the commissioning of the LHC at CERN in 2007. The luminosity increase provided by the Main Injector and Recycler, along with the upgrades of the collider detectors, will provide unique opportunities for the discovery of light Higgs bosons, supersymmetric particles and other evidence for physics beyond the Standard Model. Full exploitation of these opportunities with the CDF detector will require upgrades beyond those implemented for the first stage (Run IIa) of the Tevatron's Run II physics program. Most of the Run IIa upgrades are described in a Technical Design Report [1]. The upgraded CDF detector, including beyond-the-baseline enhancements [2], was installed in February of 2001, and is now collecting data from $p\bar{p}$ collisions at \sqrt{s} of 1.96 TeV.

Since the design of CDF's Run IIa upgrades, the long term plans for Tevatron Collider operation have evolved, projecting integrated luminosities well beyond the initial goal of 2 fb^{-1} . It is now anticipated that collection of physics data will continue until at least 15 fb^{-1} of integrated luminosity is collected by both the CDF and D0 experiments. This will result in 7.5 times the total radiation dose specified for the Run IIa CDF upgrade, and will require the replacement of the inner silicon microstrip detectors (L00 and SVXII). Furthermore, the increase in instantaneous luminosity to $5 \times 10^{32} \text{ cm}^{-2}\text{s}^{-1}$ will compromise the performance of other detector, trigger and data acquisition systems. The upgrade of these components, beyond the original Run IIa design, is referred to as the CDF IIb Project. These CDF Run IIb detector upgrades are described in this document, which will not duplicate a description of the previous upgrades described in the original CDF Run IIa Technical De-

sign Report [1].

We devote the rest of Chapter 1 to a history of CDF's data taking, a tabulation of our design goals, and a brief overview of the detector and project plan.

In Chapter 2 we motivate the detector design with a review of the physics program, extrapolating from our understanding of Run I to the prospects for Run II.

Chapter 3 describes the motivation for the need to replace the inner silicon detectors, SVX II and L00. A baseline replacement detector is proposed that meets the needs of the experiment, and establishes the scope of the project. Chapter 4 describes studies used to support the design of the baseline Run IIb silicon detector.

Chapter 5 describes the replacement of the Central Preradiator Chamber system.

Chapter 6 describes the data acquisition system with bandwidth increases needed for the Run IIb instantaneous luminosity.

Chapter 7 describes the installation scenario.

1.2 History

The Collider Detector at Fermilab (CDF) is a general purpose experiment for the study of $p\bar{p}$ collisions at $\sqrt{s} = 1.8 \text{ TeV}$ at the Fermilab Tevatron Collider. First collisions were produced and detected in October of 1985, and the Tevatron and CDF performance have evolved together to yield data sets of ever increasing sensitivity:

- $\sim 25 \text{ nb}^{-1}$ in 1987
- $\sim 4.5 \text{ pb}^{-1}$ in 1988-1989 (Run 0)
- $\sim 19 \text{ pb}^{-1}$ in 1992-1993 (Run Ia)
- $\sim 90 \text{ pb}^{-1}$ in 1994-1996 (Run Ib)

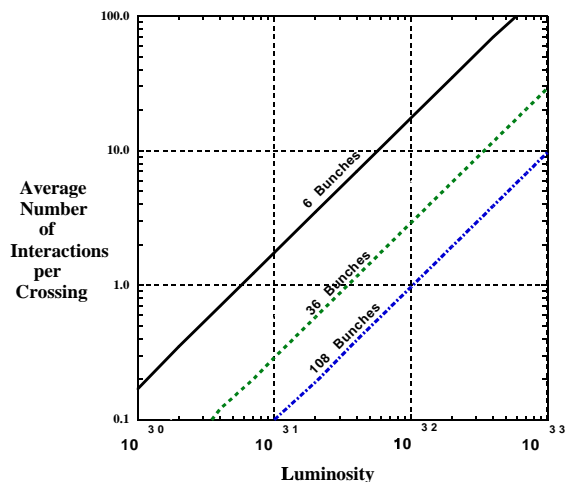


Figure 1.1: \bar{N} for various conditions at CDF. 36 bunches \equiv 396 ns crossings, 108 bunches \equiv 132 ns crossings

- $\sim 2000 \text{ pb}^{-1}$ in 2001-2004 (Run IIa, anticipated)
- $\sim 13000 \text{ pb}^{-1}$ in 2004-2007 (Run IIb, anticipated)

During the 1988 run the Tevatron met and surpassed its design luminosity of $1 \times 10^{30} \text{ cm}^{-2} \text{ s}^{-1}$. The 1994 accumulation utilized instantaneous Tevatron luminosities in excess of $2 \times 10^{31} \text{ cm}^{-2} \text{ s}^{-1}$.

The particle physics returns from this steadily evolving sensitivity include the discovery of the top quark and an accurate measurement of its mass $m_t = 176.1 \pm 6.6$, precision measurement of $m_W = 80.433 \pm 0.079 \text{ GeV}/c^2$, measurement of the inclusive jet cross section out to transverse energies of 400 GeV, precision measurement of many b hadron properties, and many of the most stringent limits on non-standard processes. The complete CDF physics archive (see Chapter 8), as of September 2001, is a collection of over 200 published papers ranging over the full state of the art in hadron collider physics.

1.3 Accelerator Configuration for Run IIb

The stated goal of Tevatron Run IIb is the accumulation of 15 fb^{-1} at $\sqrt{s} = 1.96 \text{ TeV}$, using luminosities up to $5 \times 10^{32} \text{ cm}^{-2} \text{ s}^{-1}$. This modest increase in the Tevatron energy over Run I has a significant physics benefit, (for instance increasing the $t\bar{t}$ yield by 40%)

but little impact on the detector performance. Detector issues are driven instead by the luminosity, the number of bunches, and the time between crossings. During Run IIb operation, we anticipate that the $p\bar{p}$ crossing time will be both 396 ns and 132 ns. This time structure is unchanged from the Run IIa specification, so no modifications are needed solely due to bunch spacing. The number of bunches and the luminosity together determine a key design input, \bar{N} , the average number of overlapping interactions in a given beam crossing. \bar{N} is displayed as a function of luminosity and crossing rate in Fig 1.1. The detector design for Run IIb specifies running conditions with $\bar{N} \sim 5$.

1.4 The CDF II Detector

CDF II is a general purpose solenoidal detector which combines precision charged particle tracking with fast projective calorimetry and fine grained muon detection.

The detector is shown in a solid cutaway view on the cover of this report, and in an elevation view in Fig. 1.2. Tracking systems are contained in a superconducting solenoid, 1.5 m in radius and 4.8 m in length, which generates a 1.4 T magnetic field parallel to the beam axis. Calorimetry and muon systems are all outside the solenoid. The main features of the detector systems are summarized below and described in greater detail in [1]. We use a coordinate system where the polar angle θ is measured from the proton direction, the azimuthal angle ϕ is measured from the Tevatron plane, and the pseudo-rapidity is defined as $\eta = -\ln(\tan(\theta/2))$.

1.4.1 Tracking Systems

Efficient, precision charged particle tracking is at the heart of the CDF analysis technique. To meet our physics goals we must maintain or improve the efficiency of our tracking at high luminosity.

For Run II, we have an optimized “integrated tracking system” shown schematically in Fig. 1.3. At large radii, an open cell drift chamber, the COT, covers the region $|\eta| \leq 1.0$. Inside the COT, a silicon “inner tracker” is built from two components. A microvertex detector at very small radii establishes the ultimate impact parameter resolution. Two additional silicon layers at intermediate radii provide p_T resolution and b-tagging in the forward region $1.0 \leq |\eta| \leq$

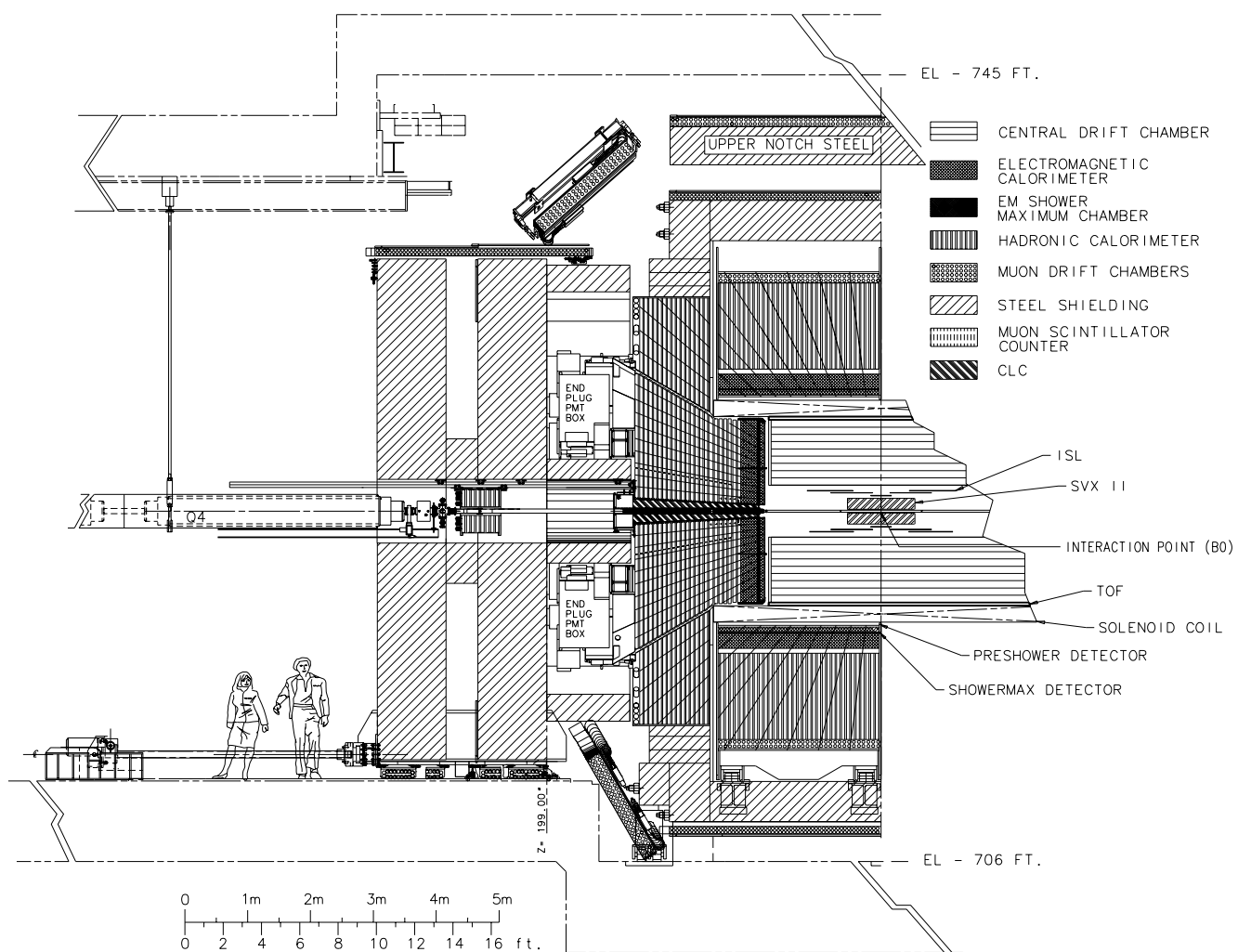


Figure 1.2: Elevation view of one half of the CDF II detector

CDF Tracking Volume

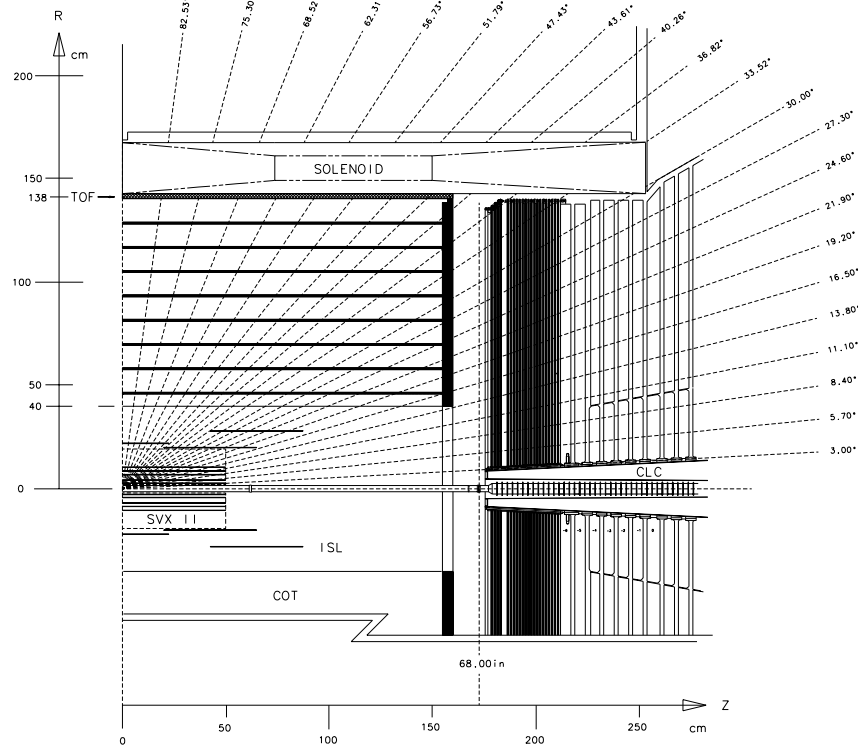


Figure 1.3: Longitudinal View of the CDF II Tracking System

2.0, and *stand-alone* silicon tracking over the full region $|\eta| \leq 2.0$.

As discussed in [1], stand-alone silicon segments allow integrated tracking algorithms which maximize tracking performance over the whole region $|\eta| \leq 2.0$. We showed there that a good signal to noise ratio for the silicon segments requires at least five measurements. In the central region, the stand-alone silicon segment can be linked to the full COT track to give excellent p_T and impact parameter resolution. Beyond $|\eta| = 1.0$, where the COT acceptance and efficiency falls precipitously, a seventh silicon layer at 28 cm is required in order to recover acceptable p_T and impact parameter resolution for a stand-alone silicon track (not segment!) in that region. These strengths of the silicon tracking system will be preserved and modestly improved by the replacement detector pro-

posed for Run IIb.

The main parameters of the integrated tracking system are summarized in Tables 1.1,1.2. The performance is benchmarked in [1].

1.4.1.1 Central Outer Tracker: COT

Tracking in the region $|\eta| \leq 1.0$ will be done with an open cell drift chamber, the COT, covering radii between 44 and 132 cm. This device will be retained for Run IIb.

The COT uses small drift cells and a fast gas to limit drift times to less than 100 ns. The basic drift cell has a line of 12 sense wires alternating with shaper wires every 3.8 mm, running down the middle of two gold-on-mylar cathode planes which are separated by ~ 2 cm. Four axial and four stereo superlayers provide

COT	
Radial coverage	44 to 132 cm
Number of superlayers	8
Measurements per superlayer	12
Readout coordinates of SLs	$+3^\circ \ 0 \ -3^\circ \ 0 \ +3^\circ \ 0 \ -3^\circ \ 0^\circ$
Maximum drift distance	0.88 cm
Resolution per measurement	180 μm
Rapidity coverage	$ \eta \leq 1.0$
Number of channels	30,240
Material thickness	1.3% X_0
ISL	
Radial coverage	20 to 28 cm
Number of layers	one for $ \eta < 1$; two for $1 < \eta < 2$
Readout coordinates	r- ϕ and r-uv (1.2° stereo) (all layers)
Readout pitch	110 μm (axial); 146 μm (stereo)
Resolution per measurement	16 μm (axial)
Total length	174 cm
Rapidity coverage	$ \eta \leq 1.9$
Number of channels	268,800
Material thickness	2% X_0

Table 1.1: Design parameters of the tracking system components common to Runs IIa and IIb.

96 measurements between 44 and 132 cm, requiring a total of 2,520 drift cells and 30,240 readout channels. The wires and cathode planes are strung between two precision milled endplates, and the complete chamber is roughly 1.3% of a radiation length at normal incidence.

The COT is currently operating in Run IIa. The detector has operated very well up to this point.

1.4.1.2 ISL: Intermediate Silicon Layers

Another section of the tracking system that will remain unchanged for Run IIb is the Intermediate Silicon Layers (ISL). In the central region, a single ISL layer is placed at a radius of 22 cm. This layer has not yet been commissioned in Run IIa, since a cooling problem has made its operation impossible. The prospects for repair of this cooling problem are not yet clear. In the plug region, $1.0 \leq |\eta| \leq 2.0$, two layers of silicon are placed at radii of 20 cm and 28 cm. SVX II and ISL together are a single functional system which provides stand-alone silicon tracking and b-tagging over the full region $|\eta| \leq 2.0$.

Double sided silicon is used with 55 μm strip pitch on the axial side and 73 μm pitch on the stereo side

with a 1.2° stereo angle. Every other strip is read out to reduce the total channel count to 268,800. Due to charge sharing through the intermediate strips, the single hit resolution perpendicular to the strip direction will be $\leq 16 \mu\text{m}$ on the axial side and $\leq 23 \mu\text{m}$ on the stereo side. The ISL readout electronics are identical to the SVX II, and will be reused for Run IIb.

1.4.1.3 SVX IIb

The design of the Run IIb inner tracker is very similar to the combination of the Run IIa SVXII plus L00, but will be more radiation tolerant and easier to build. The fundamental changes from the Run IIa design are driven by the high radiation environment of Run IIb. The SVX3D chip would not survive and is also no longer available. We are fortunate however, that technology has advanced in the intervening years and it is now standard to use a 0.25 μm process which naturally radiation hard. Design of the SVX4 chip for Run IIb began over a year ago and submission of a full chip is imminent. Details of the chip design are discussed in Chapter 3.

The double sided sensors used in SVXII are also

	SVX II/L00	SVX IIb
Radial coverage	1.3 to 10.7 cm	1.9 to 16.6 cm
Number of layers	6	6
Readout coordinates	r- ϕ on one side of all layers	r- ϕ on one side of all layers
Stereo side	none, r-z, r-z, r-uv, r-z, r-uv (uv \equiv 1.2° stereo)	none, r-z, r-z, r-z, r-uv, r-uv, r-z (uv \equiv 2.5° stereo)
Readout pitch	50-65 μ m r- ϕ ; 60-150 μ m stereo	50-88 μ m r- ϕ , 88-92 μ m stereo
Total length	87.0 cm	112.0 cm
Rapidity coverage	$ \eta \leq 2.0$	$ \eta \leq 2.0$
Number of channels	405,504	520,704
Power dissipated	3.0 KW	3.0 KW

Table 1.2: A comparison between the design parameters of the Run IIa detectors (SVX II/L00) and the baseline Run IIb silicon proposal

incapable of surviving the Run IIb radiation dosages. Here we benefit from the extensive research and development efforts that have been ongoing for the LHC experiments. The lifetime of single sided sensors is determined by the bias voltage they can withstand (at least ≈ 500 V is needed) and the temperature of the silicon. In the Run IIb design we plan to use these sensors and also actively cool the silicon.

The new silicon detector has been designed with the following constraints in mind:

- The new detector should retain or improve the tracking capability of the Run IIa detector.
- Interruption of operations should be as short as possible. Six months is the target installation period.
- The new detector must be compatible with the existing data acquisition system.
- The new detector must be compatible with the existing infrastructure; detector space, cable space, and cooling system.
- The new detector must be compatible with the Silicon Vertex Trigger (SVT), so that impact parameter triggering is not compromised.
- Little time is available for construction, so the number of parts must be kept to a minimum.

We believe that the baseline design presented in Chapter 3 meets all these criteria.

Table 1.2 shows a comparison of the Run IIa and IIb silicon detectors. Briefly, the Run IIb detector will

have 6 axial layers and two small angle stereo layers as did SVXII+L00. It also includes a set of 90° stereo layers similar to those in SVXII. In Run IIb however, the active silicon will be more evenly spaced in radius and will cover a larger area. The stereo tracking will be improved over Run IIa by reducing the pitch on the small angle and 90° sensors, using a larger angle on the small angle stereo layers and by locating a 90° layer at large radius where the occupancy is low.

The Run IIb design is fundamentally different from the Run IIa detector in that a single stave (ladder in the Run IIa language) design is used for all but the inner two layers. This will significantly simplify the construction and prototyping processes. These staves have axial sensors on one side and stereo on the other. The design is essentially independent of whether the stereo side contains 90° or small angle sensors. If further study and experience with Run IIa data indicate that the particular choice presented in Chapter 3 should change, this will not impact the schedule or the prototyping efforts already underway. The smallest layer, mounted on the beampipe, is a simplified version of the Run IIa L00 design. Because of space constraints, the layer outside the beampipe layer requires a unique stave design; the outer layer stave is too large, but it would be difficult to build another layer in the style of L00. The design presented in Chapter 3 introduces a minimum number of staves with a different design (12, compared to 156 outer layer staves) and is derived from the stave design of the outer layers.

$ \eta $ Range	$\Delta\phi$	$\Delta\eta$
0. - 1.1 (1.2 h)	15°	~ 0.1
1.1 (1.2 h) - 1.8	7.5°	~ 0.1
1.8 - 2.1	7.5°	~ 0.16
2.1 - 3.64	15°	0.2 - 0.6

Table 1.3: CDF II Calorimeter Segmentation

	Central	Plug
EM:		
Thickness	$19X_0, 1\lambda$	$21X_0, 1\lambda$
Sample (Pb)	$0.6X_0$	$0.8X_0$
Sample (scint.)	5 mm	4.5 mm
WLS	sheet	fiber
Light yield	160 pe/GeV	300 pe/GeV
Sampling res.	$11.6\%/\sqrt{E_T}$	$14\%/\sqrt{E}$
Stoch. res.	$14\%/\sqrt{E_T}$	$16\%/\sqrt{E}$
SM size (cm)	$1.4\phi \times (1.6-2.0)Z$	0.5×0.5 UV
Pre-shower size	$1.4\phi \times 65Z$ cm	by tower
Hadron:		
Thickness	4.5λ	7λ
Sample (Fe)	1 in. C, 2 in. W	2 in.
Sample (scint.)	10 mm	6 mm
WLS	finger	fiber
Light yield	~ 40 pe/GeV	39 pe/GeV

Table 1.4: Central and Plug Calorimeter Comparison

1.4.2 Calorimeter Systems

Outside the solenoid, scintillator-based calorimetry covers the region $|\eta| \leq 3.0$ with separate electromagnetic and hadronic measurements with a segmentation given in Table 1.3. The CDF calorimeters have obviously played a key role in the physics program by measuring electron and photon energies, jet energies, and net transverse energy flow. The ability to match tracks with projective towers and EM shower position in the central region has lead to a powerful analysis and calibration framework, including an understanding of the absolute jet energy scale to 2.5%.

For Run II, the existing scintillator-based central calorimeters will continue to perform well. The central and plug calorimeters both have fast enough energy measurement response times to take full advantage of the 132 ns bunch spacing. Shower maximum and pre-shower functions in the plug upgrade are also

fast enough, while the wire chamber pre-shower and shower maximum in the central system will need to integrate several bunches. The shower maximum detector in the central calorimeter is inaccessible, so this deficiency cannot be addressed in any reasonable time scale. The preshower detector will be replaced for Run IIb by a scintillator based detector with the same response time available to the plug calorimeter. A general comparison of the central and plug calorimeters is given in Table 1.4.

1.4.3 Muon Systems

CDF II uses four systems of scintillators and proportional chambers in the detection of muons over the region $|\eta| \leq 1.5$. The absorbers for these systems are the calorimeter steel, the magnet return yoke, additional steel walls, and the steel from the Run I forward muon toroids. The geometric and engineering problems of covering the full η region using these absorbers leads to the four logical systems. As seen in Table 1.5, they are all functionally similar. The CDF II tracking system provides a capability for muon momentum reconstruction over this full region of pseudorapidity.

1.4.4 Electronics and Triggering

The CDF electronics systems have been substantially altered to handle Run II accelerator conditions. The increased instantaneous luminosity requires a similar increase in data transfer rates. However it is the reduced separation between accelerator bunches that has the greatest impact, necessitating a new architecture for the readout system.

Figure 1.4 shows the functional block diagram of the readout electronics. To accommodate a 132 ns bunch-crossing time and a 4 μ s decision time for the first trigger level, all front-end electronics are fully pipelined, with on-board buffering for 42 beam crossings. Data from the calorimeters, the central tracking chamber, and the muon detectors are sent to the Level-1 trigger system, which determines whether a $\bar{p}p$ collision is sufficiently interesting to hold the data for the Level-2 trigger hardware. The Level-1 trigger is a synchronous system with a decision reaching each front-end card at the end of the 42-crossing pipeline. Upon a Level-1 trigger accept, the data on each front-end card are transferred to one of four local Level-2 buffers. The second trigger level is an asynchronous system with an average decision time of 20 μ s.

	CMU	CMP/CSP	CMX/CSX	IMU
Pseudo-rapidity coverage	$ \eta \lesssim 0.6$	$ \eta \lesssim 0.6$	$\sim 0.6 \leq \eta \lesssim 1.0$	$\sim 1.0 \leq \eta \lesssim 1.5$
Drift tube cross-section	2.68 x 6.35 cm	2.5 x 15 cm	2.5 x 15 cm	2.5 x 8.4 cm
Drift tube length	226 cm	640 cm	180 cm	363 cm
Max drift time	800 ns	1.4 μ s	1.4 μ s	800 ns
Total drift tubes (present)	2304	864	1536	none
Total drift tubes (Run II)	2304	1076	2208	1728
Scintillation counter thickness		2.5 cm	1.5 cm	2.5 cm
Scintillation counter width		30 cm	30-40 cm	17 cm
Scintillation counter length		320 cm	180 cm	180 cm
Total counters (present)		128	256	none
Total counters (Run II)		269	324	864
Pion interaction lengths	5.5	7.8	6.2	6.2-20
Minimum detectable muon p_T	1.4 GeV/c	2.2 GeV/c	1.4 GeV/c	1.4-2.0 GeV/c
Multiple scattering resolution	12 cm/p (GeV/p)	15 cm/p	13 cm/p	13-25 cm/p

Table 1.5: Design Parameters of the CDF II Muon Detectors. Pion interaction lengths and multiple scattering are computed at a reference angle of $\theta = 90^\circ$ in CMU and CMP/CSP, at an angle of $\theta = 55^\circ$ in CMX/CSX, and show the range of values for the IMU.

A Level-2 trigger accept flags an event for readout. Data are collected in DAQ buffers and then transferred via a network switch to a Level-3 CPU node, where the complete event is assembled, analyzed, and, if accepted, written out to permanent storage. These events can also be viewed by online monitoring programs running on other workstations.

1.4.4.1 Data Acquisition

A block diagram of the data acquisition system is shown in Fig. 1.5. Timing signals associated with the beam crossing are distributed to each crate by the Master-Clock subsystem. Trigger decision information is distributed by the Trigger-System-Interface subsystem. Commercial processors read data from modules in their local crate and deliver it to the VME Readout Boards (VRBs) and the Event-Building subsystem. This system concentrates the data and delivers it to the Level-3 trigger subsystem through a commercial network switch. The Level-3 trigger is a “farm” of parallel processors, each fully analyzing a single event. The Data-Logging subsystem delivers events to mass storage and also to online monitoring processes to verify that the detector, trigger, and data acquisition system are functioning correctly. Our plans for data acquisition during Run IIb are described in Chapter 6.

1.4.4.2 Trigger

In Run Ib, the trigger had to reduce the raw collision rate by a factor of 10^5 to reach < 10 Hz, an event rate that could be written to magnetic tape. With an order of magnitude increase in luminosity for Run II, the trigger must have a larger rejection factor while maintaining high efficiency for the broad range of physics topics we study.

We use a tiered “deadtimeless” trigger architecture. The event is considered sequentially at three levels of approximation, with each level providing sufficient rate reduction for the next level to have minimal dead-time. Level-1 and Level-2 use custom hardware on a limited subset of the data and Level-3 uses a processor farm running on the full event readout. The trigger, like the DAQ, is fully pipelined.

The block diagram for the CDF II trigger system is presented in Fig. 1.6. Events accepted by the Level-1 system are processed by the Level-2 hardware. The Silicon Vertex Tracker (SVT) provides, for the first time in a hadron-collider experiment, the ability to trigger on tracks with large impact parameters. This will make accessible a large number of important processes involving hadronic decay of b -quarks, such as $Z \rightarrow b\bar{b}$, $B^0 \rightarrow \pi^+\pi^-$, and exotic processes like SUSY and Technicolor that copiously produce b quarks. The Level-2 system will have improved mo-

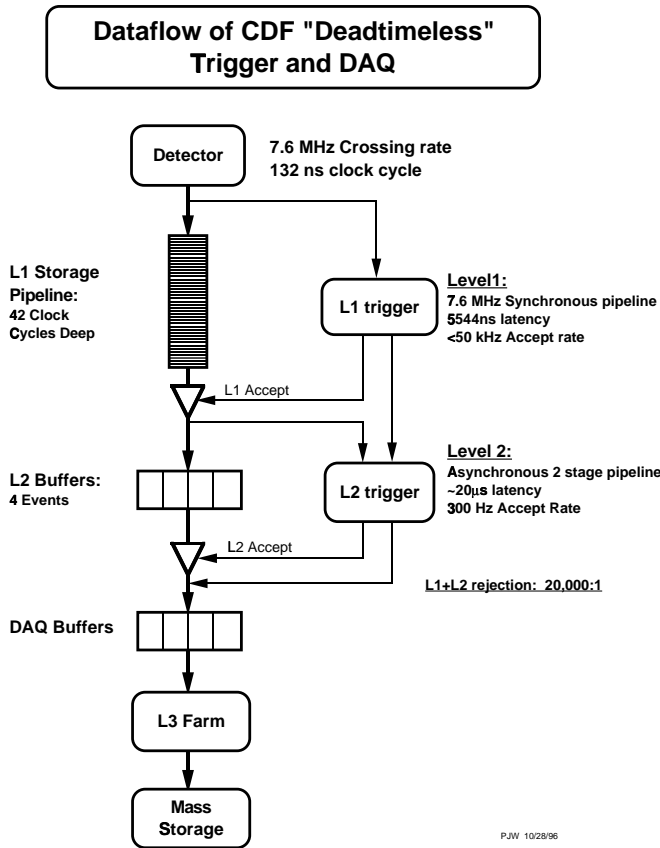


Figure 1.4: Functional block diagram of the CDF II data flow

momentum resolution for tracks, finer angular matching between muon stubs and central tracks, and data from the central shower-max detector (CES) for improved identification of electrons and photons. Jet reconstruction is provided by the Level-2 cluster finder, which, although rebuilt for the new architecture, retains the same algorithm used successfully in previous running. The Level-2 trigger is being commissioned at this time, and is not yet full operational.

The trigger system is very flexible and will be able to accommodate over 100 separate trigger selections. With a 40 kHz accept rate at Level-1 and a 1000 Hz rate out of Level-2, we expect to limit deadtime to < 10% at full luminosity, while writing events to mass storage at 30-50 Hz.

1.5 The CDF II Upgrade Plan

Our goal is to install and recommission CDF for the resumption of data taking as quickly as possible. Every effort will be made to minimize the time

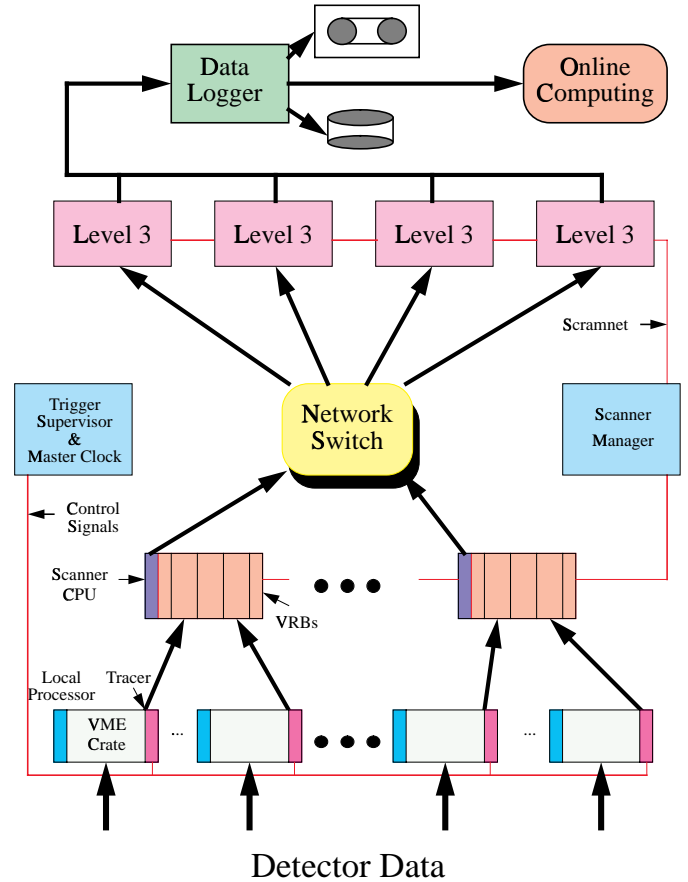


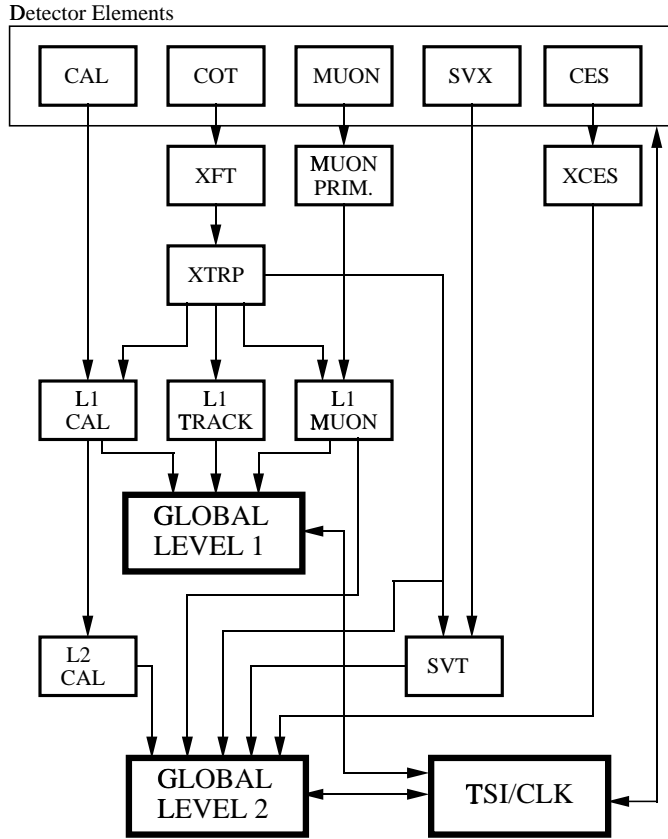
Figure 1.5: A schematic of the CDF II Data Acquisition system, showing data flow from the front-end and trigger VME crates to the Online Computing system.

that the installation of this project takes away from operations.

This document is the TECHNICAL DESCRIPTION of the baseline CDF II detector. Additional documents describe the managerial, cost, and schedule aspects of the project:

- CDF Run IIb Project Management Plan
- Memoranda of Understanding (MOU) and Work Plans for each subproject
- Cost and Schedule Plan
 - Task-based resource-loaded schedule, including labor estimates
 - Cost Estimate and Work Breakdown Structure (WBS), including contingency analysis
 - WBS Dictionary
 - Financial Plan for U.S. and non-U.S. funding

RUN II TRIGGER SYSTEM



PJW 9/23/96

Figure 1.6: Block diagram of the CDF II trigger system.

1.5.1 Outlook

The baseline scope of the detector proposed here meets every goal for a rejuvenated detector capable of operations with the Tevatron + Main Injector at $\mathcal{L} = 5 \times 10^{32} \text{cm}^{-2}\text{s}^{-1}$, 132 ns bunch spacings, and to last through 15fb^{-1} of integrated luminosity.

- The tracking system will be a fully optimized combination of drift chamber and silicon with powerful redundancy that insures excellent pattern recognition, momentum resolution, and b-tagging out to $|\eta| = 2$, even in the presence of multiple interactions.
- The calorimetry will be exclusively scintillator based, fast, and have resolution equal to or better than the existing detector.

- The muon system will have almost full azimuthal coverage in the central region, and expanded coverage out to $|\eta| = 2.0$.
- The electronics will be fully compliant with 132 ns or 396 ns bunch crossing in every channel, and the data acquisition system and Level-3 trigger will be capable of 1000 Hz operation.
- The trigger will be deadtimeless, ready for every crossing, with tracking information at Level-1 and impact parameter discrimination at Level-2.

This design reflects the accumulated experience of a decade of physics with CDF at the Tevatron. With CDF II and anticipated data sets in excess of 15fb^{-1} in Run II, we look forward to major discoveries at Fermilab in the years to come.

Bibliography

- [1] “The CDF II Detector Technical Design Report”,
The CDF II Collaboration, FERMILAB-Pub-
96/390-E, November 1996.

Chapter 2

Physics Goals

2.1 Overview

In this chapter we will describe the physics goals of the CDF II experiment, and the connection between the physics and the detector design. Our physics plan includes six complementary lines of attack on the open questions of the Standard Model:

- search for a light Higgs boson
- characterization of the properties of the top quark
- a global precision electroweak program
- direct search for new phenomena
- tests of QCD at large Q^2
- constraint of the CKM matrix with B hadrons

This physics program is comprehensive in its methods and its scope. It has classic precision measurements, such as m_W and α_s , taken to a new level of accuracy; it has a survey of newly discovered territory, in the first complete study of the top quark; and it extends our reach for new phenomena into a regime where current theoretical speculation suggests new structure. We believe that the power of the CDF II detector combined with the sensitivity of the Run II data sets will result in a significant advance in our understanding of the behavior of elementary particles, if not outright discovery of physics beyond the Standard Model.

In this chapter we will justify this claim. We begin with a summary of our conclusions and then turn to each of the six topics in detail. Since the CDF II experiment re-uses or extends many of the same detector technologies and strategies as its predecessor, the physics analyses of Run II will employ many of the techniques refined during Run I. The physics

projections and detector specifications will therefore frequently appeal to a brief review of the current status. We note that our conclusions have the power of direct extrapolations from a well tuned device in a well measured environment.

Table 2.1 shows the expected yields for some benchmark processes with 15 fb^{-1} of Tevatron collisions recorded by the CDF II detector. These are the numbers of identified events available for offline analysis. The statistical precision of Run II, combined with capability of the CDF II detector, will provide rich programs of measurement in each of the six sub-fields, summarized below.

2.1.1 Higgs Boson Physics

The origin of electroweak symmetry breaking is one of the most fundamental questions in elementary particle physics. One explanation is the existence of Higgs bosons. Fits to precision electroweak data suggest that one of the Higgs bosons should be light (below $200 \text{ GeV}/c^2$), and the minimal supersymmetric model requires a Higgs boson with mass less than about $130 \text{ GeV}/c^2$. These facts make the search for light Higgs bosons one of the most important goals of experimental elementary particle physics. The CDF and D0 experiments have the opportunity to make this discovery in Tevatron Run II. This search directly drives our plan to upgrade the CDF detector to a configuration that will operate with B tagging capabilities at instantaneous luminosities of $5 \times 10^{32} \text{ cm}^{-2} \text{ s}^{-1}$ and integrated luminosities approaching 30 fb^{-1} . The details of the Tevatron search strategy for a light Higgs boson have been explored in a Fermilab Higgs Workshop [2]. A brief summary of this workshop and the CDF plans for Higgs boson searches are presented in Section 2.2.

Mode	Yield (15 fb ⁻¹)
TOP	
dilepton	1125
$W + 3j * b$	6750
$W + 4j * b$	5440
$W + 4j * bb$	1350
VECTOR BOSONS	
$W \rightarrow l\nu$ (e, μ)	32M
$Z \rightarrow l^+l^-$ (e, μ)	4.5M
$W\gamma, W \rightarrow e\nu$	30K
$Z\gamma, Z \rightarrow e^+e^-$	13.5K
$W^+W^- \rightarrow l\nu l\nu$	1500
$W^+Z^- \rightarrow l\nu ll$	375
QCD	
$j + X, \eta \leq 1.0, E_T \geq 300$ GeV	48K
$jj + X, M_{jj} \geq 600$ GeV	225K
$\gamma + X, p_T(\gamma) \geq 25$ GeV	45M
$\gamma\gamma + X, p_T(\gamma_1, \gamma_2) \geq 12$ GeV	105 K
$W + \geq 1j, E_T(W) \geq 100$ GeV	75K
$Z + \geq 1j, E_T(Z) \geq 100$ GeV	7.5K
B	
$B^0 \rightarrow J/\psi K_S$	150K
$B^0 \rightarrow \pi^+\pi^-$	38K
$B_s \rightarrow J/\psi\phi$	60K

Table 2.1: Representative yields for known processes, after selection. We use the CDF Run I selections modified for increased coverage of the CDF II detector (see text) and we assume 2.0 TeV collisions. $j \equiv$ jet, and $j * b \equiv$ b-tagged jet.

2.1.2 Properties of the Top Quark

A sample of almost 7,000 b-tagged, identified events will allow a detailed survey of the properties of the top quark. A review of this program is given in Section 2.3.

The top mass will be measured with a precision conservatively estimated to be 2.0 GeV/ c^2 . The total cross section will be measured to 6%, and non-standard production mechanisms will be resolvable down to total cross sections of ~ 90 fb. The branching fraction to b quarks will be measured to 1%, decays to non-W states may be explored at the level of 3%, and branching ratios to the various W helicity states will be measured with uncertainties of order 1%. The magnitude of any FCNC decay will be probed down to branching fractions of 0.5% or less. We will isolate the

electroweak production of single top, allowing a cross section measurement with an uncertainty of 12%, and inference of $|V_{tb}|$ with a precision of 6%.

The final top physics program will undoubtedly be richer than this list, which should be interpreted as a catalog of probable sensitivities for the baseline top survey and whatever surprises the top may have in store.

2.1.3 A Precision Electroweak Program

The study of the weak vector bosons at the Tevatron is anchored in the leptonic decay modes. The new plug, intermediate muon system and integrated tracking will give triggerable electron coverage out to $|\eta| = 2.0$, triggerable muon coverage out to $|\eta|$ of at least 1.2 and taggable muon coverage out to $|\eta| = 2.0$. This will double the number of $W \rightarrow e\nu$ events and *triple* the acceptance for Z's and dibosons in the electron and muon channels. A data set of 15 fb⁻¹ in combination with the acceptance and precision of the CDF II detector results in the comprehensive program in electroweak physics discussed in detail in Section 2.4.

One of our main goals is the measurement of m_W with a precision of ± 20 MeV/ c^2 . The combined precision on m_W and m_{top} will allow inference of the Standard Model Higgs mass m_H with precision of 30%.

The W decay width, Γ_W will be measured to 15 MeV, a factor of twelve improvement on the LEP-II expectation. The precision on A_{FB} at the Z^0 pole will be sufficient to improve on the measurement of $\sin^2\theta_W^{eff}$ over LEP and SLD results, and measurement off the pole will be sensitive to new phenomena at high mass scales. Limits on anomalous WWV and ZZ γ couplings, bolstered by the forward tracking and lepton identification, will surpass those of LEP-II. The W charge asymmetry measurement, also augmented by unambiguous lepton ID in the plug region, will provide much improved constraints on parton distribution functions.

2.1.4 Search for New Phenomena

The CDF II experiment will search for new objects at and above the electroweak scale. There is at present a great deal of theoretical activity focussed on new phenomena in this regime, with predictions from models invoking supersymmetry, technicolor, and new U(1) symmetries. The magnitude of the top quark mass

and speculation about an excess in the top cross-section have led to other theoretical predictions about phenomena well within our reach in Run II, such as topcolor. Search strategies for these and other models are discussed in Section 2.5.

We will be sensitive to charginos up to 130 GeV/ c^2 , to gluinos up to 270 GeV/ c^2 , and to stop squarks up to 150 GeV/ c^2 . Second generation lepto-quarks can be observed up to masses of 300 GeV/ c^2 , new vector bosons can be probed up to masses of 900 GeV/ c^2 , and excited quarks up to 800 GeV/ c^2 . Quark compositeness can be observed up to a scale of approximately 5 TeV. These are all model dependent limits, and, as in the case of the top survey above, we believe that our catalog of prospects here is best interpreted as a list of probable sensitivities for the real surprises waiting at the electroweak scale.

2.1.5 Precision QCD at Large Q^2

The QCD sector of the Standard Model will be stringently tested using the production and fragmentation properties of jets, and the production properties of W/Z bosons, Drell-Yan lepton pairs, and direct photons. We will evaluate the precision of QCD calculations beyond leading order (higher order perturbative calculations and soft gluon resummation corrections), and determine the fundamental input ingredients, namely parton distribution functions and the running coupling constant α_s .

The precision of QCD measurements at CDF II with 15 fb $^{-1}$ will provide sensitivity to many sources of new physics. For example, the strong coupling constant α_s will be measured over the entire range $(10's \text{ GeV})^2 < Q^2 < (500 \text{ GeV})^2$, and deviations from the Standard Model running could signal loop contributions from new particles. A direct search for the substructure of quarks at the level of 10^{-19} m will be possible with high E_T jets and the production angular distribution of di-jets. Finally a broad range of searches will be carried out for the decays of massive particles to various combinations of jets, W/Z bosons, photons and neutrinos via missing E_T .

2.1.6 Constraining the CKM Matrix

CDF II plans to take advantage of the copious production of the various species of b hadrons at the Tevatron to make measurements which will test the consistency of the Standard (CKM) Model of weak quark mixing

and CP violation. By extending the capabilities developed in Run I into Run II, CDF II expects to be able to measure CP asymmetries in $B^0 \rightarrow J/\psi K_S$ and $B^0 \rightarrow \pi^+\pi^-$ decays with a precision comparable to the e^+e^- colliders. Complementary information will come from a sensitive search for CP violation in $B_s \rightarrow J/\psi\phi$ decays. The effects of mixing in the $B_s^0 - \bar{B}_s^0$ system will be measured, allowing a determination of the ratio of CKM elements $|V_{td}/V_{ts}|$ over the full range allowed by the Standard Model.

In addition CDF II will continue to improve the precision on measurements of b hadron decay properties (*e.g.* B^0 vs. B^+ lifetimes) and pursue the observation and study of rare decays (*e.g.* $B^0 \rightarrow K^{*0}\mu^+\mu^-$). The physics of heavier b hadrons, for instance B_c , will be the exclusive domain of the Tevatron collider for at least the next decade. An overview of CDF II expectations for B physics in Run II is given in Section 2.7.

2.1.7 Detailed Discussion

The scientific prospects for CDF II are discussed in the following sections of this chapter.

The physics opportunities provide much of the rationale for the CDF II design choices, and the discovery prospects detailed here underscore our excitement about completing this upgrade and returning to high luminosity data taking at the Tevatron Collider as quickly as possible.

2.2 Higgs physics in Run 2b

The search of the origin of electroweak symmetry breaking is the central question in high energy physics today. The most recent fits to the world's combined electroweak data[1] favor the existence of a Standard-Model-like Higgs with mass in the range 100-200 GeV. The lower limit on the Higgs mass from the LEP2 experiments is 113.4 GeV; the data from all four experiments show a 2-sigma excess at a Higgs mass of about 115 GeV.

The Tevatron experiments have the opportunity, in the years before the LHC turns on, to search for the Higgs both in the Standard Model (SM) and in supersymmetry, using a variety of search channels discussed here. The Run 2b upgrades, and in particular the replacement for the Run 2a silicon vertex detector, are crucial to carrying out this physics program.

2.2.1 Standard Model Higgs

Events with a SM scalar Higgs can be produced at the Tevatron in several ways. The most copious production mode is gluon-gluon fusion via a heavy quark loop, giving a single Higgs produced. The Higgs can also be produced in association with a W or Z boson via its couplings to the vector bosons. Figure 2.1 shows the production cross section for various modes as a function of Higgs mass.

Figure 2.2 shows the branching ratios of the Standard Model Higgs as a function of Higgs mass. In the range below about 135 GeV Higgs mass, the decay to $b\bar{b}$ dominates, and for larger masses the decay to W pairs dominates.

In the gluon fusion case, for low mass Higgs, there is an overwhelming background from QCD production of $b\bar{b}$ pairs. The WH and ZH modes, however, have been extensively studied[2] and lead to several distinct signatures in which a Higgs signal can be observed with sufficient integrated luminosity.

2.2.2 Low-mass Higgs

For low mass (< 135 GeV) Higgs, the most sensitive signatures arise from the leptonic decays of the W and Z , and are denoted $\ell\nu b\bar{b}$, $\nu\bar{\nu} b\bar{b}$, and $\ell^+\ell^- b\bar{b}$. Hadronic decays of the W and Z lead to the $q\bar{q}b\bar{b}$ final state which suffers from large backgrounds from QCD multi-jet production.

In Run 1 in CDF, all four of these channels were studied, and led to limits on the Higgs cross section

times branching ratio to $b\bar{b}$ as depicted in Figure 2.3. As the plot shows, the Run 1 limits are more than an order of magnitude above the expected Standard Model cross section, naturally provoking the question of whether and how this search can be carried out in Run 2.

Improvements to the detector, coupled with much higher instantaneous luminosity in Run 2 lead to greatly enhanced sensitivity in the Standard Model Higgs search. Unlike the Run 1 detector, the CDF Run 2 detector has a silicon vertex detector covering the entire luminous region, and has measurements of the z coordinates of tracks. Overall, the tracking coverage out to nearly $|\eta| = 2$ and the new muon chambers lead to greatly improved acceptance for Higgs. For the missing E_T channel ($\nu\bar{\nu}b\bar{b}$) channel, the trigger efficiency can be improved by using the silicon vertex trigger (SVT) to tag the jets. Coupled with the fact that the accelerator is expected to deliver a data sample over a hundred times larger than that in Run 1, the overall sensitivity of the Higgs search is dramatically improved in Run 2.

Beyond the improvements to the detector itself, maximizing the sensitivity of the search for the Higgs depends most critically on attaining the best possible $b\bar{b}$ mass resolution, and attaining the best possible b jet tagging efficiency and purity, and understanding and controlling the main irreducible backgrounds from vector boson plus heavy flavor production.

In Run 1 the top quark discovery and subsequent determination of its mass demonstrated that one could use jet information, even jets from b quarks, which have a significant semileptonic branching ratio, to determine the top mass. The case of the Higgs is simpler than that of the top, which suffers from large combinatorics. For the Higgs, the mass resolution is limited by basic physics (missing energy from neutrinos and gluon radiation) and detector resolution.

The benefit of making corrections for missing neutrinos is illustrated by CDF's search in Run 1 for $Z \rightarrow b\bar{b}$. Figure 2.4 shows the successive effects of correcting for overall missing energy, and muon p_T , and more general jet energy corrections. The mass resolution attained in this analysis was 13.5%; for a 120 GeV Higgs (in the background-dominated process $Z \rightarrow b\bar{b}$) the resolution predicted is 12%.

One can improve upon the jet energy corrections employed in most Run 1 analyses by making the best possible use of all detector information, including tracking, shower max, calorimeter, and muon cham-

bers. Figure 2.5 shows the improvement to jet energy resolution possible by determining jet energy from an optimum linear combination of all jet information. Using all information results in a 30% improvement in jet energy resolution.

A great deal of simulation and calibration work remains and is presently underway. Optimistically, by putting together all the best kinematic corrections with optimal jet energy corrections, we hope to eventually achieve 10-12% mass resolution for the Higgs in the main low-mass search channels. (This is not as good as the $Z \rightarrow b\bar{b}$ case because there is additional missing energy in the Higgs channels due to neutrinos from W and Z decay.)

Figure 2.6 shows the raw mass distribution and Figure 2.7 shows the background-subtracted signal in the $\ell\nu b\bar{b}$ case, for a 120 GeV SM Higgs, combining data from both CDF and D representing 15 fb^{-1} integrated luminosity, assuming a 10% $b\bar{b}$ mass resolution, which is what was assumed (optimistically) in the Tevatron Run 2 Higgs report. The figure clearly illustrates that even with the best resolution attainable, discovering the Higgs remains a major challenge.

2.2.3 High-mass Higgs

For larger Higgs masses ($> 135 \text{ GeV}$), the Higgs decays predominantly to $WW^{(*)}$. Two modes have been shown[2] to be sensitive in this mass range: $\ell\nu\bar{\ell}\nu$ (from gluon fusion production of single Higgs) and $\ell^\pm\ell^\pm jj$ (from tri-vector-boson final states).

The critical issues in these search modes are accurate estimation of the very large ($\sim 10 \text{ pb}$) WW background in the $\ell\nu\bar{\ell}\nu$ case and channel and estimation of the $t\bar{t}$ and W/Z +jets backgrounds in the like-sign dilepton channel.

2.2.4 SM Higgs Reach in Run 2

The integrated luminosity required to discover or exclude the Standard Model Higgs, combining all search channels and combining the data from CDF and D, is shown in figure 2.8. The lower edge of the bands is the nominal estimate of the Run 2 study, and the bands extend upward with a width of about 30%, indicating the systematic uncertainty in attainable mass resolution, b tagging efficiency, and other parameters.

The figure clearly shows that discovering a SM (or SM-like) Higgs at the 5-sigma level requires a very large data sample: even with 15 fb^{-1} , the mass reach is about 120 GeV at best. A 95% CL exclusion can,

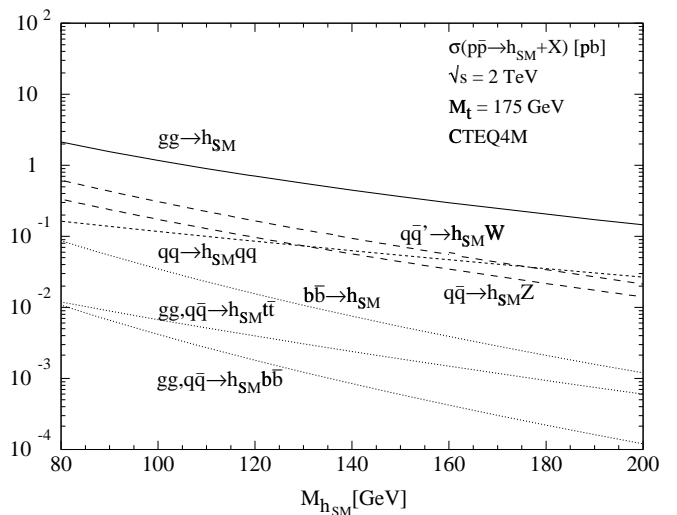


Figure 2.1: Production cross section for Standard Model Higgs at the Tevatron as a function of Higgs mass.

however, be attained over the entire mass range 115-190 GeV with the integrated luminosity foreseen in Run 2b.

The $b\bar{b}$ mass resolution assumed in making these estimates is 10% in the central part of the distribution. This represents a significant improvement over the 14-15% resolution achieved in this analysis in Run 1, which did not benefit from the more detailed corrections described above and developed after the analysis was completed. A great deal of effort, presently underway, is needed to understand the jet energy corrections to the level required to attain 10% resolution. The required integrated luminosity for Higgs discovery scales linearly with this resolution.

The estimates of required integrated luminosity assume that the b tagging efficiency and purity are essentially the same as in Run 1 in CDF, per taggable jet. The better geometric coverage of the Run 2a and 2b silicon systems, however, is taken into account and leads to a much larger taggable jet efficiency. Since the required integrated luminosity scales inversely with the *square* of the tagging efficiency (assuming constant mistagging rates), however, there is a potentially great payoff for developing high-efficiency algorithms for b -tagging. Any such algorithms depend crucially on the quality of the information coming from the silicon vertex tracking system; the Run 2b silicon system has indeed been designed to optimize the performance in high- E_T b jet tagging.

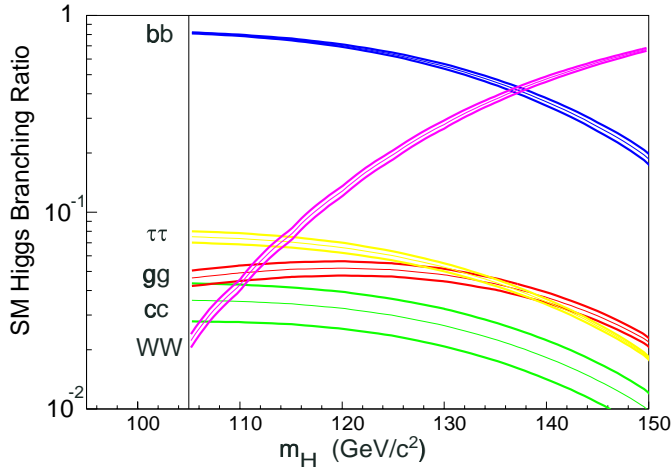


Figure 2.2: Branching ratios for Standard Model Higgs.

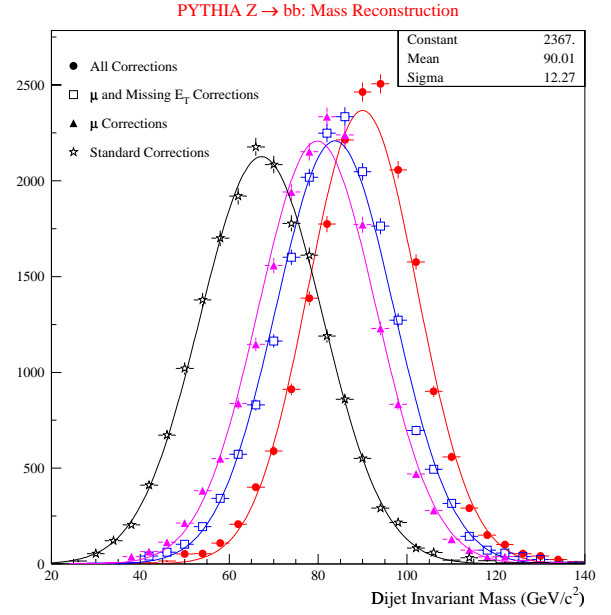


Figure 2.4: Mass resolution improvement for $Z \rightarrow b\bar{b}$ events as successive corrections are applied. After all corrections the resolution is 12%.

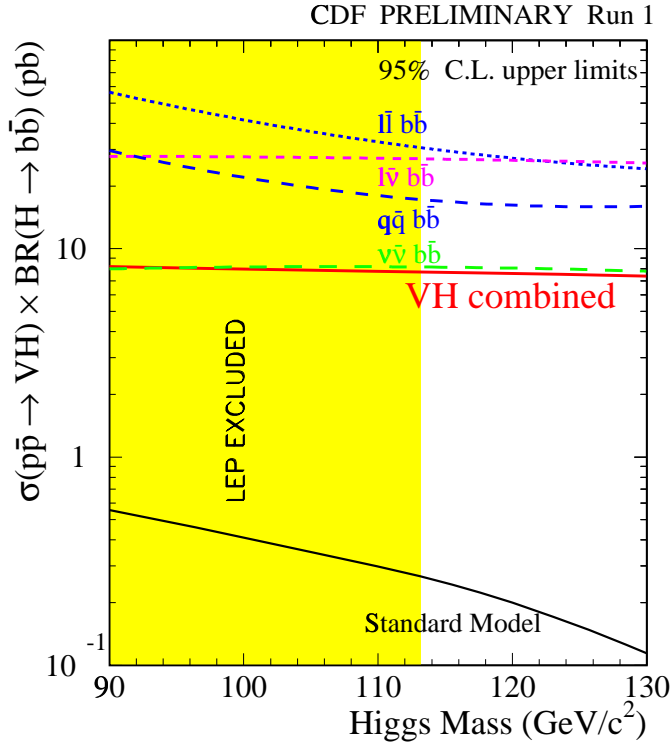


Figure 2.3: Limits on SM Higgs cross section times branching ratio to $b\bar{b}$ from CDF in Run 1.

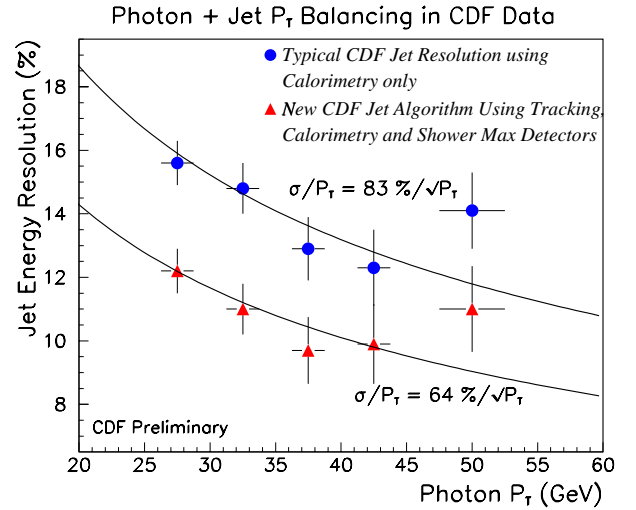


Figure 2.5: Jet energy resolution as a function of jet E_T , comparing standard corrections based on calorimeter only with energy determination combining information from tracking detectors, calorimetry, and shower max.

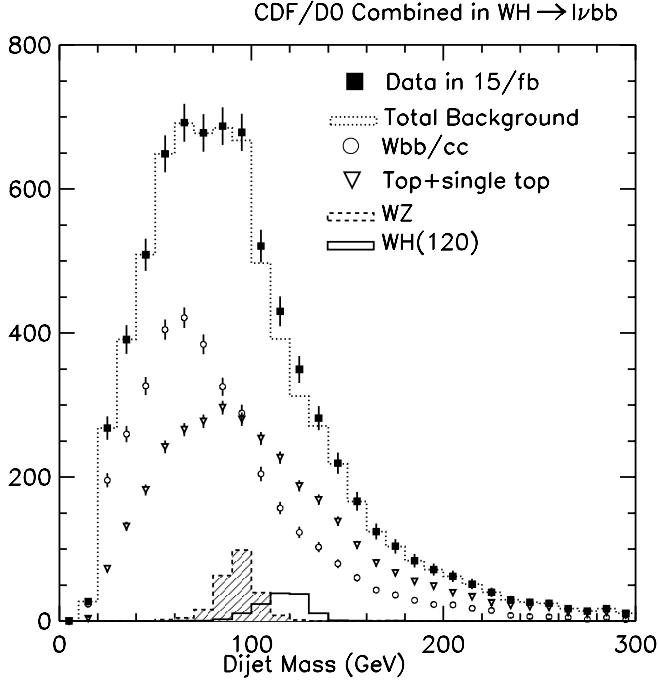


Figure 2.6: Distribution of $b\bar{b}$ mass in the $\ell\nu b\bar{b}$ Higgs search channel, showing expected background sources and expected signal from 120 GeV SM Higgs, combining 15 fb^{-1} of data from CDF and D.

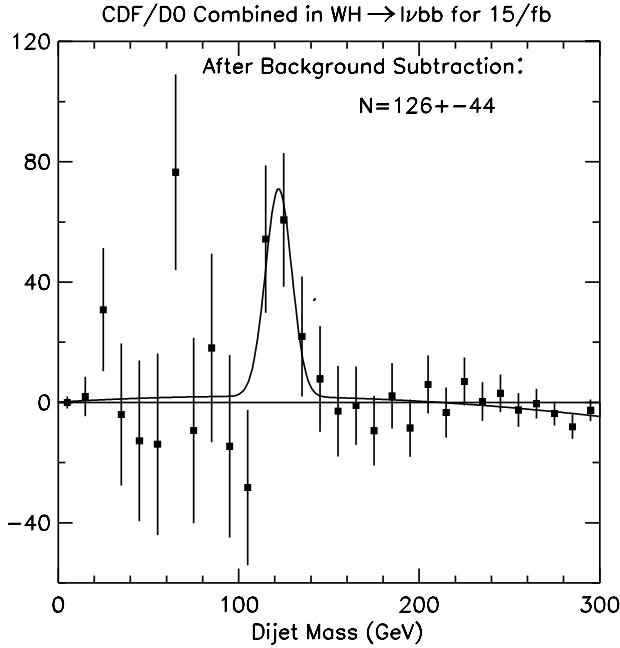


Figure 2.7: Background subtracted $b\bar{b}$ mass distribution in the $\ell\nu b\bar{b}$ channel, showing expected signal from 120 GeV SM Higgs, combining 15 fb^{-1} of data from CDF and D.

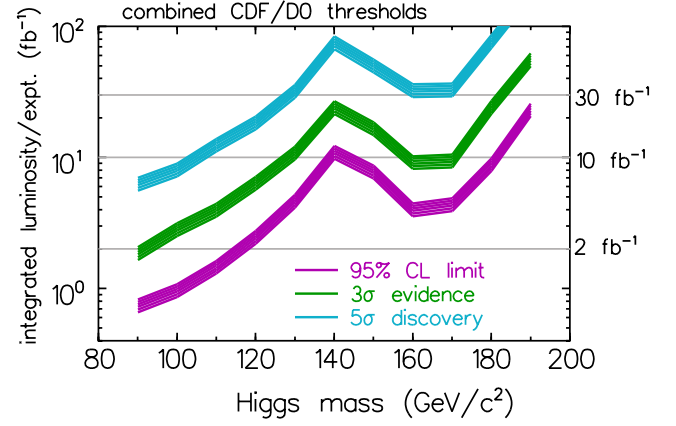


Figure 2.8: The integrated luminosity required per experiment to either exclude a SM Higgs boson at 95% CL or discover it at the 3σ or 5σ level, as a function of the Higgs mass. These results are based on the combined statistical power of both CDF and D and combining all search channels.

2.2.5 SUSY Higgs

In the context of the minimal supersymmetric standard model (MSSM) the Higgs sector has two doublets, one coupling to up-type quarks and the other to down-type quarks and leptons. There are five physical Higgs boson states, denoted h , A , H , and H^\pm . The masses and couplings of the Higgses are determined by two parameters, usually taken to be m_A and $\tan\beta$ (the ratio of the vacuum expectation value of the two Higgs doublets), with corrections from the scalar top mixing parameters.

The light scalar h can appear very Standard-Model-like or nearly so over a larger range of MSSM parameter space. In this scenario the results of the search for the SM Higgs produced in the WH and ZH modes are directly interpretable. Figure 2.9 shows the range in the space of m_A versus $\tan\beta$ in which a 5-sigma discovery can be made, as a function of integrated luminosity, for one choice of stop mixing.

More interesting is the case of large $\tan\beta$. Since the coupling of the neutral Higgses ($h/A/H$) to down-type quarks is proportional to $\tan\beta$, there is an enhancement factor of $\tan^2\beta$ for the production of $b\bar{b}\phi$, $\phi = h, A, H$ relative to the SM rate appearing in figure 2.1. This leads to distinct final states with four b jets; if we demand that at least three of the jets be tagged, the background from QCD multijet processes is relatively small. In Run 1, CDF searched for this process, and from the null result excluded a

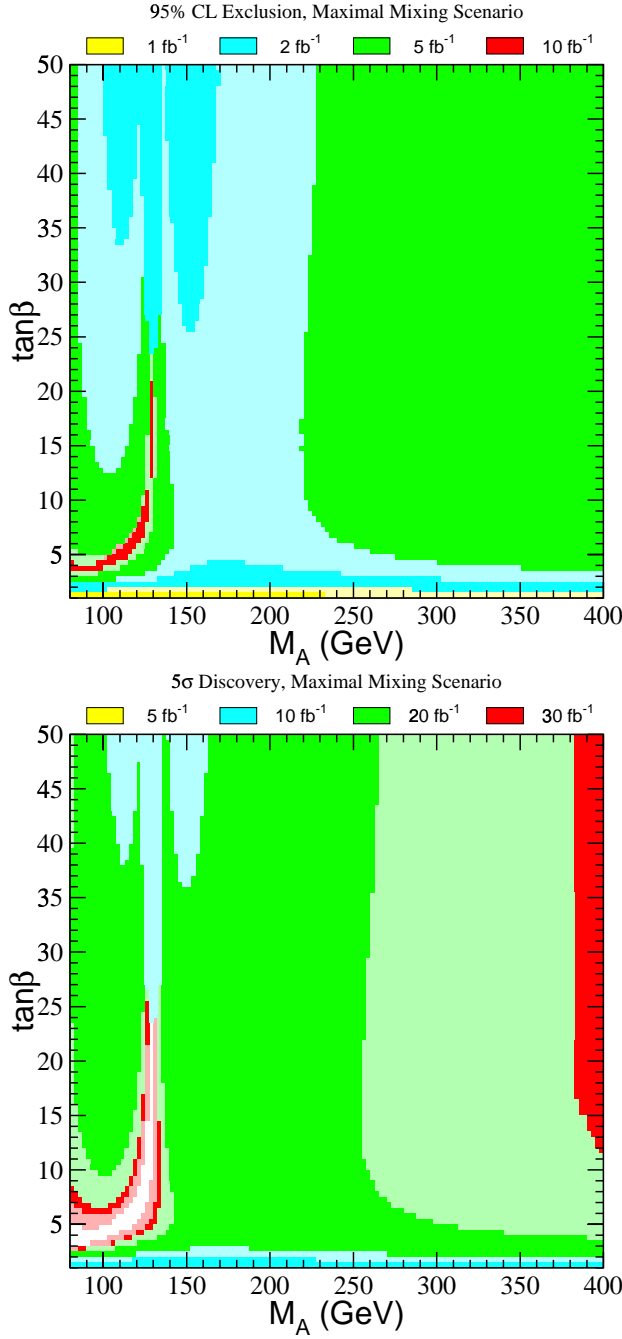


Figure 2.9: Regions of MSSM Higgs parameter space where 95% exclusion can be attained (above) and where 5σ discovery is possible (below), using SM Higgs search results.

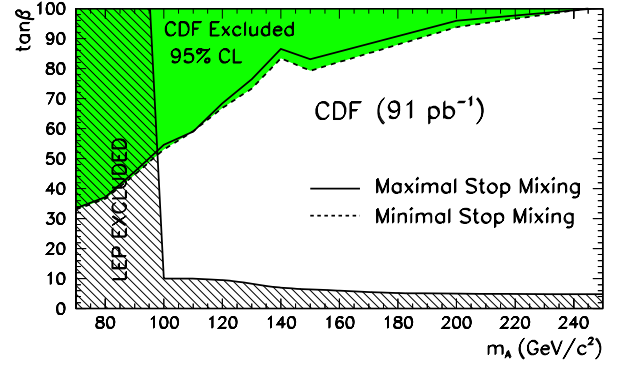


Figure 2.10: CDF limits on MSSM Higgs using $b\bar{b}b\bar{b}$ final state.

large swath of MSSM parameter space inaccessible to LEP, as shown in figure 2.10.

Based on the Run 1 analysis, and taking into account the improved b -tagging efficiency, Figure 2.11 shows the regions of m_A versus $\tan\beta$ that CDF can cover for different integrated luminosities. It is interesting to note that the sensitive region in this analysis includes the region which is difficult to cover using the results of the SM Higgs search (shown in Figure 2.8). For this analysis the Run 2b silicon vertex system plays an absolutely crucial role: the accepted signal rate is proportional to the cube of the b tagging efficiency!

2.2.6 Summary

With an upgraded detector and more than an order of magnitude larger instantaneous luminosity the CDF experiment, combined with D, has a significant chance of discovering a SM (or SM-like) Higgs boson in Run 2. If the Higgs mass is larger than about 130 GeV, the experiment is sensitive to the WW decay modes in two main channels. The experiment also has the chance to discover the Higgs in the MSSM, if $\tan\beta$ is large, via the striking four- b -quark final state.

The key experimental issues are maintaining the excellent secondary vertex tagging efficiency throughout the run, and working hard to understand and improve the dijet mass resolution. Clearly the physics motivation for the Run 2b upgrade to the silicon vertex system is strong, and without it this physics cannot be addressed at all.

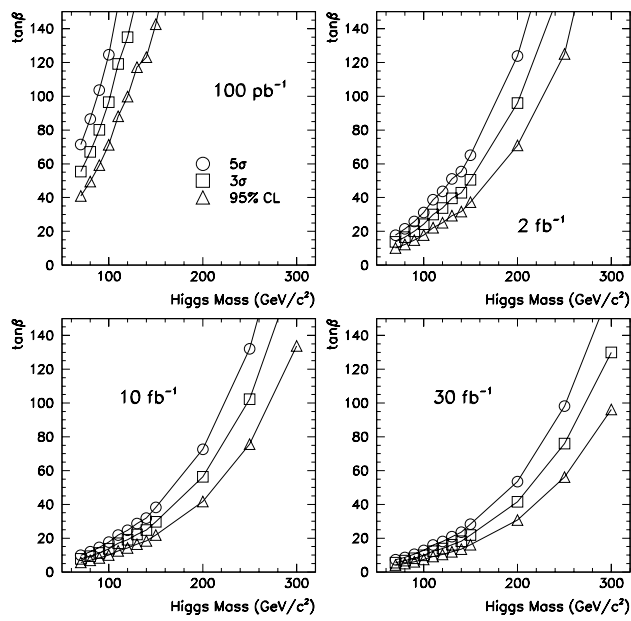


Figure 2.11: Anticipated limits in the plane of $\tan\beta$ versus $m(A)$ using $b\bar{b}b\bar{b}$ final state.

Bibliography

- [1] LEP Electroweak Working Group at CERN (see <http://lepewwg.web.cern.ch/LEPEWWG/>).
- [2] Report of the Higgs Working Group of the Tevatron Run 2b SUSY/Higgs Workshop, M. Carena *et al.*, eds., unpublished. (See hep-ph/9910338 at the LANL preprint server.)

2.3 Properties of the Top Quark

The top quark, with mass $\sim 175 \text{ GeV}/c^2$, is strongly coupled to the electroweak symmetry breaking mechanism, and decays to a real W and a b -quark before hadronizing. A program to characterize the properties of this unconventional fermion is an obvious scientific priority. The accessibility of the top quark at the Fermilab Tevatron, in conjunction with the planned luminosity and detector upgrades for Run II, creates a new arena for experimental particle physics at an existing facility, and we should fully exploit this unique opportunity over the next decade.

Tevatron Run I brought the discovery of the top quark, the first direct measurements of its mass and cross section [2, 3, 4], and valuable first experience in top quark physics. We established techniques to identify b -quark jets using secondary vertices and soft leptons from the decays $B \rightarrow \ell \nu X$ as well as establish the essential utility of b -tagging in the isolation of the top signal. We established techniques for the accurate measurement of the mass and decay kinematics of a heavy object in final states with jets, and the essential utility of *in situ* jet calibration techniques. We have explored a variety of other measurements, all of them presently limited by statistics. [44, 47, 48, 49, 50, 51, 52, 53, 54, 55, 56, 57, 45]

Armed with this experience, we have just embarked on Run IIa, a new physics program with an expected delivered luminosity of 2 fb^{-1} here at the Tevatron [1]. With this data in hand, we expect to make significant contributions to our current understanding of the top quark as discussed in the Run II Technical Design Report (TDR) [35].

This document takes as a basis the Run II TDR but takes it one step further by examining the top quark physics potential with 15 fb^{-1} worth of data. We will show that the CDF IIb detector will be capable of a complete characterization of the main properties of the top quark, and we will establish the probable precisions that can be achieved using 15 fb^{-1} of Tevatron collider data.

Since Run IIa is still in its infancy, we are not currently able to report any new physics results. Instead, we begin by reviewing the top analysis results of Run I. Next, we discuss the impact of the detector upgrade components on the top physics of Run IIb. Finally we describe the Run IIb top physics program, including yields, the mass measurement, production properties, branching ratios, and decays.

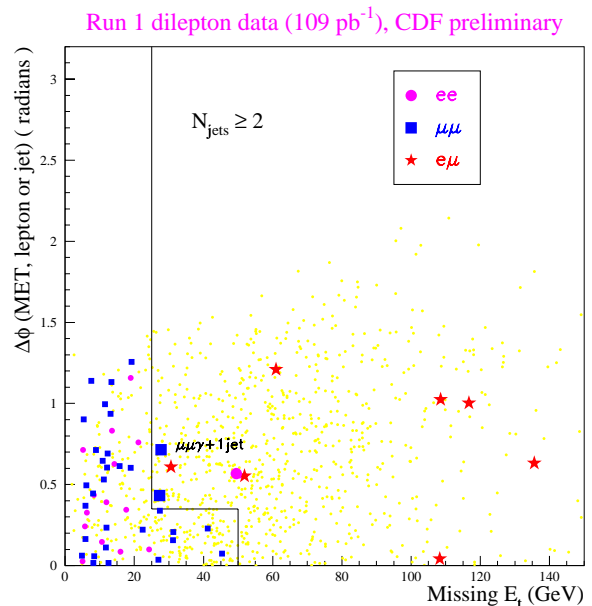


Figure 2.12: $\Delta\phi$ vs. \cancel{E}_T in the dilepton sample. The small grey dots are the result of a $t\bar{t}$ Monte Carlo simulation with $m_{\text{top}} = 175 \text{ GeV}/c^2$.

2.3.1 Review of Run I Analysis

Using 19.3 pb^{-1} from Run Ia, CDF presented initial evidence for the top quark in the spring of 1994 [2]. A year later, with an additional 48 pb^{-1} from Run Ib, CDF confirmed its original evidence for the top quark [3]. Upon completion of Run I in 1996, CDF wrote a series of papers describing the current state of understanding of the top quark utilizing the 105 pb^{-1} Run I dataset. We summarize here the results of those first measurements in this new area of physics.

2.3.1.1 Dilepton Mode

In the standard model, the t and \bar{t} -quarks both decay almost exclusively to a W -boson and a b -quark. In the “dilepton” channel, both W ’s decay leptonically ($W \rightarrow \ell \nu$), and we search for leptonic W decays to an electron or a muon. The nominal signature in this channel is two high- P_T leptons, missing transverse energy (from the two ν ’s), and two jets from the b -quarks. Acceptance for this channel is small, mostly due to the product branching ratio of both W ’s decaying leptonically (only about 5%). In the 105 pb^{-1} from Run I, CDF observed 7 $e\mu$ events, 2 $\mu\mu$ events, and 1 ee event. Figure 2.12 shows the 10 candidate events in the parameter space $\Delta\phi$ (the angle between the \cancel{E}_T and the nearest lepton or jet) vs

\cancel{E}_T (the missing transverse energy) as well as where one would expect top to lie. The background estimate for the dilepton channel is 2.4 ± 0.4 events[3]. Although not an *a priori* part of the search, we examine the jets in dilepton events for indications that they originated from b -quarks. In the 10 dilepton events, we find 6 jets in 4 events (1 $\mu\mu$ and 3 $e\mu$) which are identified (“tagged”) as b -jets. This provides evidence for b -quarks produced in association with two W ’s, as expected from the decay of a $t\bar{t}$ pair.

CDF has also investigated top decays involving the τ -lepton. We have searched for dilepton events with one high- p_T electron or muon and one hadronically decaying τ -lepton which is identified using tracking and calorimeter quantities[7]. As in the $e\mu$, ee , or $\mu\mu$ channel two jets from b -quarks and significant missing transverse energy are required. Due to the additional undetectable τ -neutrino, the τ hadronic branching ratio and the lower efficiency for τ identification, the acceptance in this channel is considerably smaller than in the case of $e\mu$, ee , or $\mu\mu$. In 105 pb^{-1} we expect about 1 event from $t\bar{t}$ and 2 events from background. We observe 4 candidate events (2 $e\tau$ and 2 $\mu\tau$). There are 4 jets in 3 candidate events that are identified as b -jets (“tagged”). More data with excellent tracking will enable us to conclusively establish this “all 3rd generation” decay mode of the top quark, which is important for charged Higgs searches and tests of weak universality.

2.3.1.2 Lepton + Jets Mode

In this channel, one of the W ’s decays leptonically to either an electron or muon (plus neutrino) and the other W decays hadronically to a pair of quarks. The nominal signature is a lepton, missing transverse energy (the neutrino from the leptonic W decay), and four jets; two from the b -quarks and two from the decay of the W . Approximately 30% of the $t\bar{t}$ events have this decay signature. Our lepton+jets selection requires that a leptonic W decay be accompanied by at least three central ($|\eta| < 2.0$) jets for an event to be considered part of the sample.

The background from W +multijet production is large. However, $t\bar{t}$ events contain two b -quark jets, and these can be distinguished from gluon and light quark jets in the background using two b -quark tagging techniques. The first technique locates a displaced vertex using the silicon-vertex detector (SVX Tag). The second locates a low- P_T electron or muon

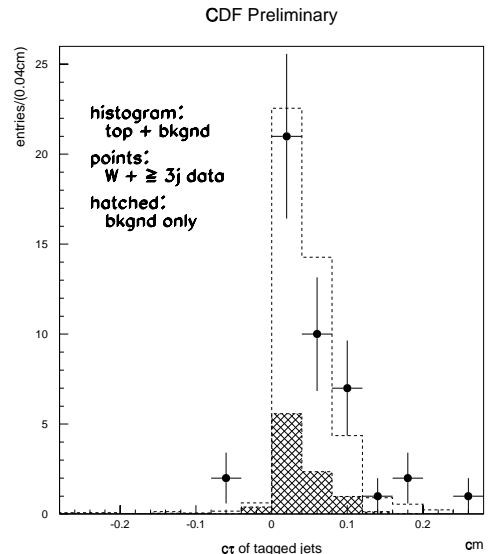


Figure 2.13: The proper time distribution for the b -tagged jets in the signal region ($W \geq 3$ jets). The open histogram shows the expected distribution of b ’s from $175 \text{ GeV}/c^2$ $t\bar{t}$ Monte Carlo simulation. The shaded histogram indicates the background in W +jet events.

primarily from the semileptonic decay of a b -quark or sequential c -quark (SLT Tag). The efficiency for tagging a $t\bar{t}$ event is $(43 \pm 4)\%$ and $(20 \pm 3)\%$ for the SVX and SLT algorithms, respectively. In 105 pb^{-1} , 37 SVX tags are observed in 29 events. The background, in the 29 SVX tagged events, is estimated from a combination of data and Monte Carlo simulation to be 8.0 ± 1.1 events. Using the SLT tagging algorithm, 44 tags are found in 40 events. The background here is estimated to be 25.2 ± 3.8 events. The two samples have 10 events in common[3]. Figure 2.14 (upper left) shows the jet multiplicity spectrum for the SVX b -tags and the background.

In the 1 and 2-jet bins, we expect little contribution from $t\bar{t}$ events. The predicted background and the observed number of events agree well in the 1-jet bin, and agree at the 1.5 sigma level in the 2-jet bin as well. In the 3 and ≥ 4 -jet bins, a clear excess of tagged events is observed. Fig. 2.13 shows the proper time distribution expected for b -tagged jets in the signal region (≥ 3 jets), compared with that for the SVX b -tagged jets in the data: the tagged jets are consistent with b decays.

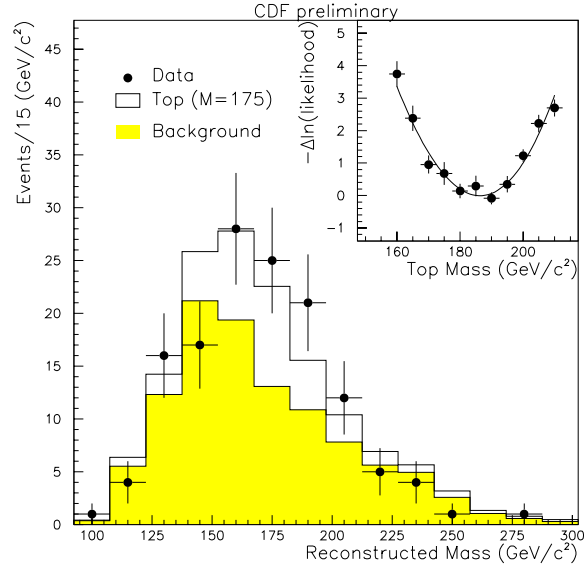
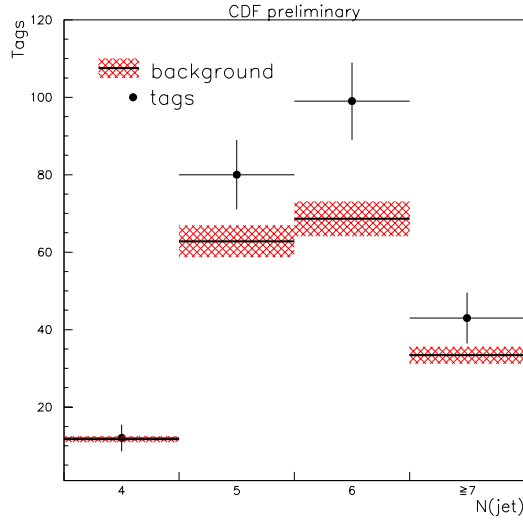
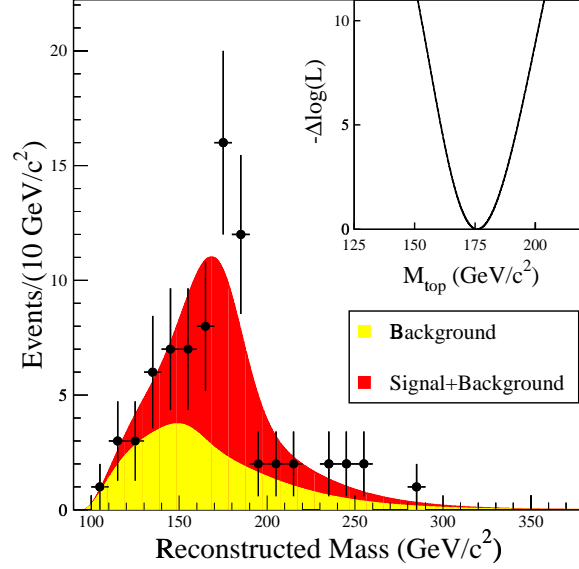
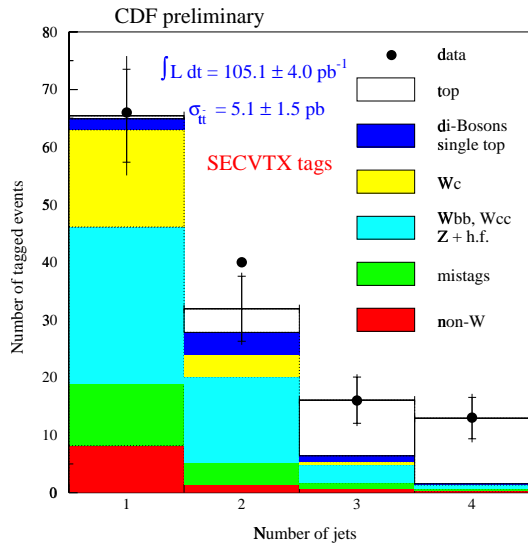


Figure 2.14: **Top Left:** The jet multiplicity distribution in SVX tagged W+jet events. Closed circles are are number of b -tagged events in each bin and shaded areas are the background prediction for the number of tagged events and its uncertainty. **Top Right:** Mass spectrum using the optimized mass sample in lepton+jet events using 105 pb^{-1} of data. The yellow (light) shaded area is the expectation from background. The red shaded area (dark) is the expectation for background plus top production. The points are the data. The likelihood fit is shown as an inset. **Bottom Left:** The jet multiplicity distribution for the all-hadronic mode. The dark circles represent the observed number of b -tags in each jet multiplicity bin and the hatched areas represent the background prediction as well as its estimated uncertainty. **Bottom Right:** Mass spectrum for all-hadronic b -tagged events in 105 pb^{-1} of data. The shaded area is the expectation from background. The histogram is from background plus top production. The likelihood fit is shown as an inset.